


Article

Erosion Behavior of API X120 Steel: Effect of Particle Speed and Impact Angle

Paul C. Okonkwo ¹, Mostafa H. Sliem ¹, Mobbassar Hassan Sk ¹, Rana Abdul Shakoor ^{1,*},
Adel Mohamed Amer Mohamed ² , Aboubakr M. Abdullah ¹ and Ramazan Kahraman ³

¹ Center for Advanced Materials (CAM), Qatar University, Doha 2713, Qatar; pauloke@yahoo.com (P.C.O.); mostafa@qu.edu.qa (M.H.S.); Skmobba@qu.edu.qa (M.H.S.); bakr@qu.edu.qa (A.M.A.)

² Department of Metallurgical and Materials Engineering, Faculty of Petroleum and Mining Engineering, Suez University, Suez 43721, Egypt; adel.mohamed25@yahoo.com

³ Department of Chemical Engineering, Qatar University, Doha 2713, Qatar; ramazank@qu.edu.qa

* Correspondence: shakoor@qu.edu.qa

Received: 1 August 2018; Accepted: 15 September 2018; Published: 26 September 2018



Abstract: The dry erosion behavior of API-X120 pipeline steel was investigated, under the erosive interaction of aluminum oxide particulates, in a range of speed (43–167 m·s⁻¹) and impact angle (30°–90°). Erosion behavior is characterized by surface profile measurement, weight loss measurement, and surface morphology analysis by SEM/EDX. Optical profilometry revealed that the eroded area increased with elevating speed of particles while the penetration depth increased with the increases in impact angle as well as particle speed. Percent weight loss and normalized erosion rate indicated that the lower impact angles and higher speeds led to higher materials loss and erosion. SEM analyses on various combinations of impact angles and particle speeds demonstrated the predominant erosion mechanism under those specific conditions; attributed to the intensity of the resolved components of the momentum vector horizontal or normal to the target metal surface under those conditions.

Keywords: erosion; particle speed; angular impact; API X120 steel; metal cutting

1. Introduction

For decades, pipeline systems have been used for transporting petroleum products [1–3]. Plain carbon steels are commonly used for constructing long-distance pipelines due to its mechanical durability and low cost [4,5]. These pipelines are often subjected to severe erosion due to the presence of a broad range of erodent particles, often found in the petroleum products [6,7]. The erosion causes mechanical removal of the surface scale, leaving the surface directly exposed to impact induced stress and accordingly degradation [8].

Erosion phenomena often occur in conjunction with corrosion. Simultaneous erosion-corrosion process is much complex. However, characterizing the erosion alone is useful to understand the standalone effects of erosion in the overall damage mechanism of pipelines. In general, the erosion behaviours of pipeline steels under different environmental conditions are available in the literatures [4,5,9]. Some of these studies have focused on understanding the erosion mechanisms of pipeline materials at different particles speeds and impact angles [10–14]. Most of these works however focused on plain carbon steels [10–12,15,16]. The results obtained from these works showed that the microstructure and the mechanical properties of target steel influence the erosion mechanism of plain carbon steels. Levy [17] investigated the erosion behavior of two plain carbon steels (AISI 1020 and 1075) at various particles speeds and impact angles using SiC solid particulates. The results indicated that the observed erosion mechanisms depend more on the characteristics of the target steels rather than erodent particles. In a

similar study, Green et al. [18] showed the erosion behaviour of another plain carbon steel (AISI 1050) of various microstructures. The result revealed that under normal temperature range the steel with martensitic microstructure behaves better than pearlitic steel due to its higher hardness. Liebhard and Levy [19] studied the influence of the erodent particle shapes on the erosion of plain carbon AISI 1018 steel. The result showed that angular particles caused higher order of erosion compared to spherical particles.

Significant efforts have been made to improve the erosion resistance of the pipeline steel over the years [17,20]. Results indicated that micro-alloying of plain carbon steels with elements, which can form a small amount of carbide and nitrate has significantly enhanced the erosion resistance of the plain carbon steels [17]. Micro-alloying of plain carbon steels with specific elements and appropriate process control (e.g., heat-treatment) provides higher hardness and strength to the ordinary plain carbon steels [21,22]. Examples of few such steels used for pipeline application are API X70, API X80, and API X100 [23–25].

In the recent times, TransCanada fabricated API X120 steel which is considered to be the highest quality pipeline steel available in today's market [26,27]. The erosion behaviour of API X120 steel has not yet been investigated in details. Available literatures provide little information about the erosion behaviour of this target material as functions of particle speed, microstructure, temperature, etc. However, it would be essential to understand the erosion mechanism of this steel under the conditions of practical interest. Understanding the interactions of API X120 steel with various erodent particles at different impact angles and velocities would be worthwhile in order to mitigate the erosion induced failures. This study focuses on investigating the effects of particle speeds and impact angles on the erosion mechanism of API X120 steel under the conditions of practical interest which are practically found inside the pipelines.

2. Materials and Methods

The target material used for the erosion tests were machined from API X120 steel sheet (Hebei Yineng Pipeline Group Co., Ltd., Jinan, China). The test specimens were 22 mm × 21 mm × 10 mm and approximate weight of 38.48 g were wet grinded to 4000 grit surface finish with silicon carbide papers, degreased in acetone, washed, dried and then stored inside a desiccator (SANPLATEC Corporation, Osaka, Japan) in order to keep the sample away from moisture before they are exposed to the actual experimental conditions. The hardness value of 253.8 HV was measured using CLC-200R Rockwell hardness machine (Clark Instruments, SUN-TEC Corporation, London, UK), while the chemical composition (Table 1) of the test material was determined using an optical emission spectrometer (OES), ARL 3460 (Thermo Fisher Scientific, Waltham, MA, USA). It is known that erosion behavior is governed not only the hardness, but also more factors such as elasticity and fracture toughness. However, the effect of the other mechanical properties is going to be studied in other studies.

Table 1. Chemical composition of target steel (API X120) and impinging solid particles.

Material	Specimen	Chemical Composition								
		C	Mn	Si	Ni	Cr	Mo	Cu	V	Fe Bal.
API X120 steel	Target material (wt.%)	0.129	0.541	0.101	0.017	0.039	0.0013	0.015	0.025	
Aluminum oxide	Impinging solid particles (wt.%)	Al ₂ O ₃ 99.4		TiO ₂ 0.01	SiO ₂ 0.051	Fe 0.079		MgO 0.022		Alkali 0.29

Distribution of the aluminum oxide particles API X120 steel samples is shown in Figure 1a. The average size of the erodent particle was ~60 μm. Representative microstructure of the as-received API X120 steel is shown in Figure 1b. Although the microstructure appeared to be a mixture of ferrite/pearlitic/martensitic phases, it still requires further detailed examination. Surface characteristics of the eroded specimen were investigated using scanning electron microscope (SEM), energy disperse spectroscopy (EDX) and 2D surface profilometry techniques.

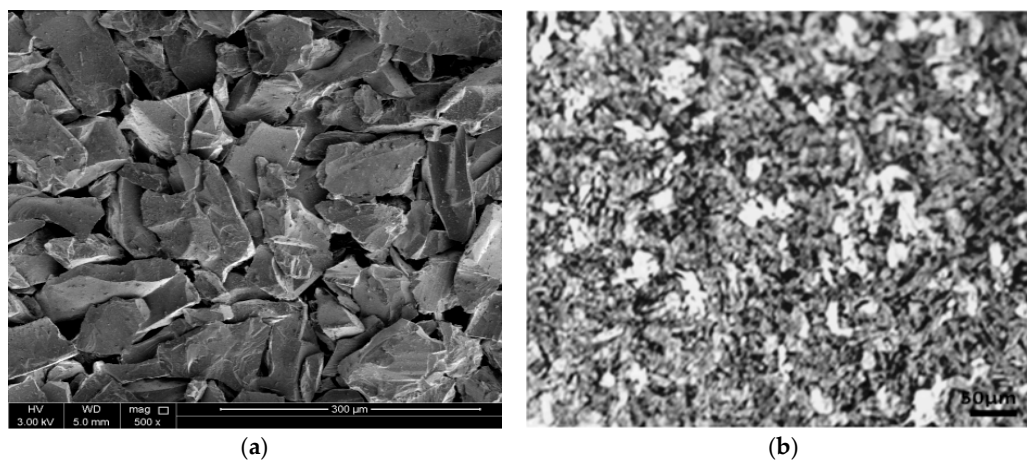


Figure 1. SEM micrographs of (a) aluminum oxide particle size distribution, (b) microstructure of the target materials (API X120).

Figure 2 shows the schematic of the setup used for performing the erosion tests per ASTM G76 [28]. This setup allows regulating the erodent particles in terms of particle velocity, particle flux and distance between the specimen surface and outlet nozzle. The working distance between the nozzle outlet and the surface of the specimen was kept constant (10 mm). A sand hopper capable of storing erodent particles is mounted directly above the sample holder. The samples were mounted on the sample holder facing the nozzle. A pneumatic vibrator was attached to the sand hopper to enhance free flow of the particles to the abrasive chamber. The mass flow rate was adjusted by controlling the speed of sand conveyor and the pressure at the vibrator. Aluminum oxide particles were fed into the venture suction from the sand hopper under pressurized air. The angle of impact of the particles were changed by adjusting the angle twister, while the air flow control switch was used to set the desired particle speed. In order to investigate the effect of particle speed on the erosion mechanism of the test specimen; the speed of the erodent particles was determined by double-disc approach [29]. This approach is preferred over the other approaches [30,31] because it allows regulating the particle speed by directly adjusting the gas pressure. In order to stabilize the feed rate, the erosion machine is turned on 30 min before the actual test. During each test, the specimen was exposed to the particle flow for a certain period of time. The dry erosion tests were performed at different particle speeds ($43\text{--}167\text{ m}\cdot\text{s}^{-1}$) and incident angles ($30^\circ\text{--}90^\circ$) in order to investigate the effects of particle speed and impact angle on the erosion behavior of API X120 steel.

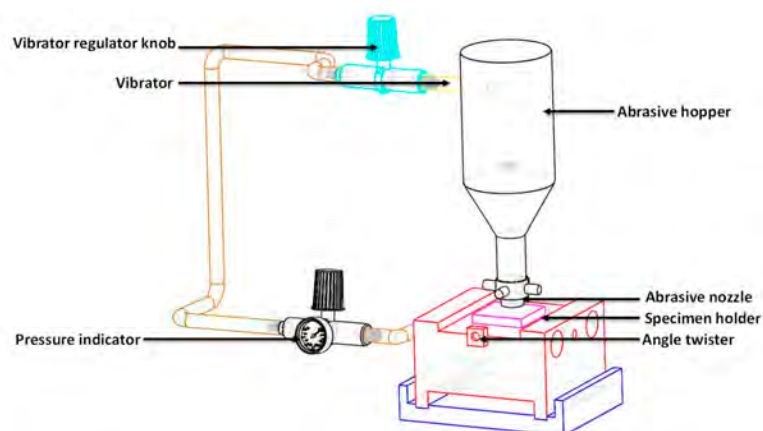


Figure 2. Schematic of the erosion machine used to study the erosive wear behavior of API X120 steel [25].

Following the same approach from our previous work [25,32–34], the feed rate of the particles was determined by measuring the weight of the abrasive particles coming through the nozzle per unit time. In order to compare the weight change as a result of the impact, each specimen was weighed before and after each test using a high precision digital balance with a precision range in the order of 10^{-6} g [35].

3. Results and Discussion

The effects of impact angles and speeds of the erodent particles on the erosion behavior were characterized by measuring the surface profile, percent weight loss, erosion rate and also by analyzing the surface morphology. A brief summary of the results is provided in Table 2.

Table 2. The effect of changing the impact angle and the particle speed on the morphology and the erosion rate of API X120 steel.

Impact Angles on the Sample Surface (°)	Particle Speed (m·s ⁻¹)	Profilometric Spread and Depth			Predominant Morphological Change Observed from SEM (Predominant Erosion Mechanism)	Normalized Erosion Rate (mg/g)
		X mm	Y mm	Z μm		
30	43	3.1	6.2	10.1	Micro-forging	0.58
	67	4.4	8.4	25.3	Superficial embedment of Al ₂ O ₃	1.30
	92	5.0	10.1	39.5	Deep embedment of Al ₂ O ₃	1.91
	167	5.3	13.2	58.6	ploughing (sideways squeezing of metals)	2.20
45	43	3.4	5.3	53.2	Micro-forging	0.41
	67	4.9	6.3	66.4	Deep embedment of Al ₂ O ₃	0.90
	92	5.4	8.2	87.2	Metal cutting	1.20
	167	6.2	10.5	98.1	Metal cutting	1.39
60	43	3.7	4.2	100	Plastic deformation and dimple formation	0.40
	67	5.0	5.1	124	Embedment of Al ₂ O ₃	0.50
	92	5.2	6.3	148	metal cutting	0.80
	167	6.6	8.3	160	Flattening of the ridges and cracks	0.95
90	43	4.1	3.1	150	Plastic deformation and dimple formation	0.21
	67	6.9	3.9	170	Plastic deformation and dimple formation	0.45
	92	8.2	5	210	Deep embedment of Al ₂ O ₃	0.46
	167	9.5	6.1	240	Flattering ridge and squeeze out	0.47

Figure 3 shows the optical profilometry of the eroded surfaces of the API X120 steels at the different impact angles. For any particular impact angle, the lateral spread (along X and Y) of the impacted region as well as the penetration depth (along Z, normal to the plane of the paper) of the impinging particles increased with increasing particle speed. Penetration depth clearly increased with increasing impact angle as well as increasing particle speed.

Figure 4 shows the weight loss percentage = [(initial wt. – final wt.)/initial wt.] × 100% profile vs. time for the four different impact angles. The weights of APIX 120 specimens measured before and after each erosion test. In order to ensure the reproducibility of the results, each type of test was repeated thrice. Weight loss percentage increased with decreasing impact angle, indicating higher materials loss at lower angular impact.

Figure 5a shows the normalized erosion rates vs. particle speed for various impact angles. Normalized erosion rates were calculated through dividing weight loss (g) by abrasive particle consumption (mg). For a particular impact angle, normalized erosion rate increased with particle speed. This observation is in agreement with Söderberg et al. [36] and Hutching et al. [37] who observed greater material removal from the target specimen surface at higher particle speed and ascribed that to the high kinetic energy associated with the high speed particles.

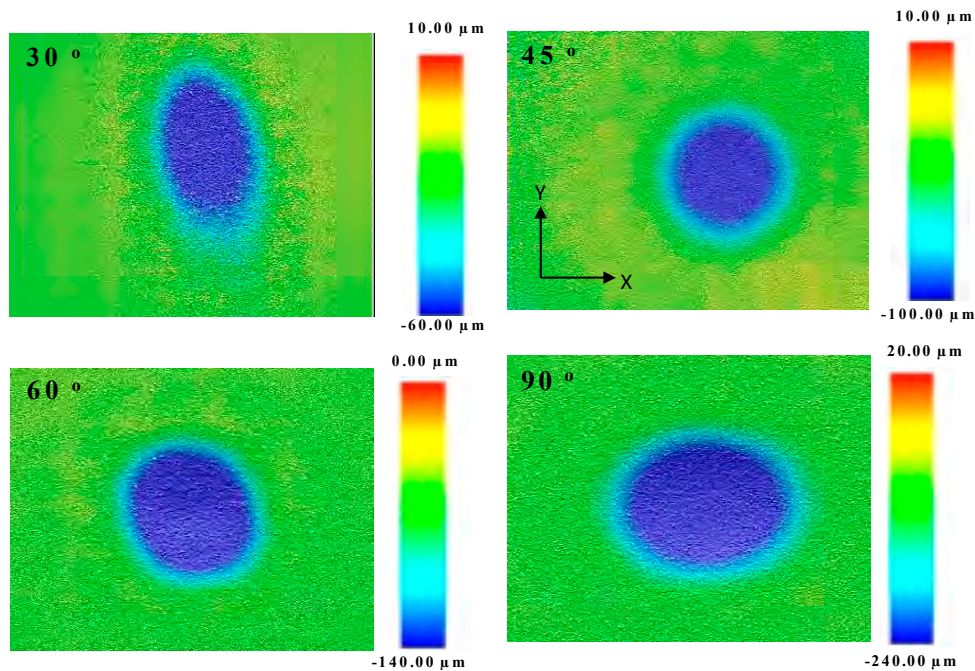


Figure 3. Representative optical profilometry of API X120 steel eroded surfaces at four different impact angles at particle speed $167 \text{ m}\cdot\text{s}^{-1}$. X and Y directions are shown, Z direction is vertically down. Features shown here are not to the scale.

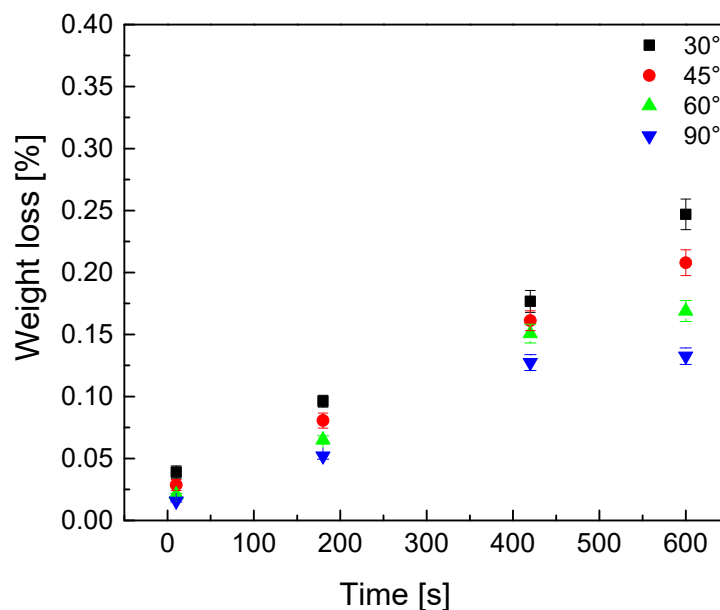


Figure 4. Weight loss of API X120 steel specimen with time. Each data point indicates average of 3 tests at each condition. Error bars indicates 1 sigma scatter.

Figure 5b illustrates normalized erosion rate vs. impact angle for various particle speeds. The effect of impact angle on the erosion rate was found to be most pronounced at 30° . High erosion rate of API X120 steel at lower impact angles is a typical characteristic of ductile materials [12,38,39]. This can however be attributed to higher value of the resolved part of the momentum vector along the metal surface (i.e., the horizontal component) at the lower impact angles compared to the higher impact angles. For any particular impact angle, higher particle speed resulted higher erosion rate. At lower particle speeds, only few particles possess enough kinetic energy to deform the surface of

the target specimen plastically. Therefore, at lower particle speeds, the target metal surface shows predominant elastic deformation. Increasing the particle speed transforms the deformation process from elastic to plastic by causing more number of erodent particles gaining higher kinetic energy. As a result of enhanced plastic deformation the erosion rate also become higher [40].

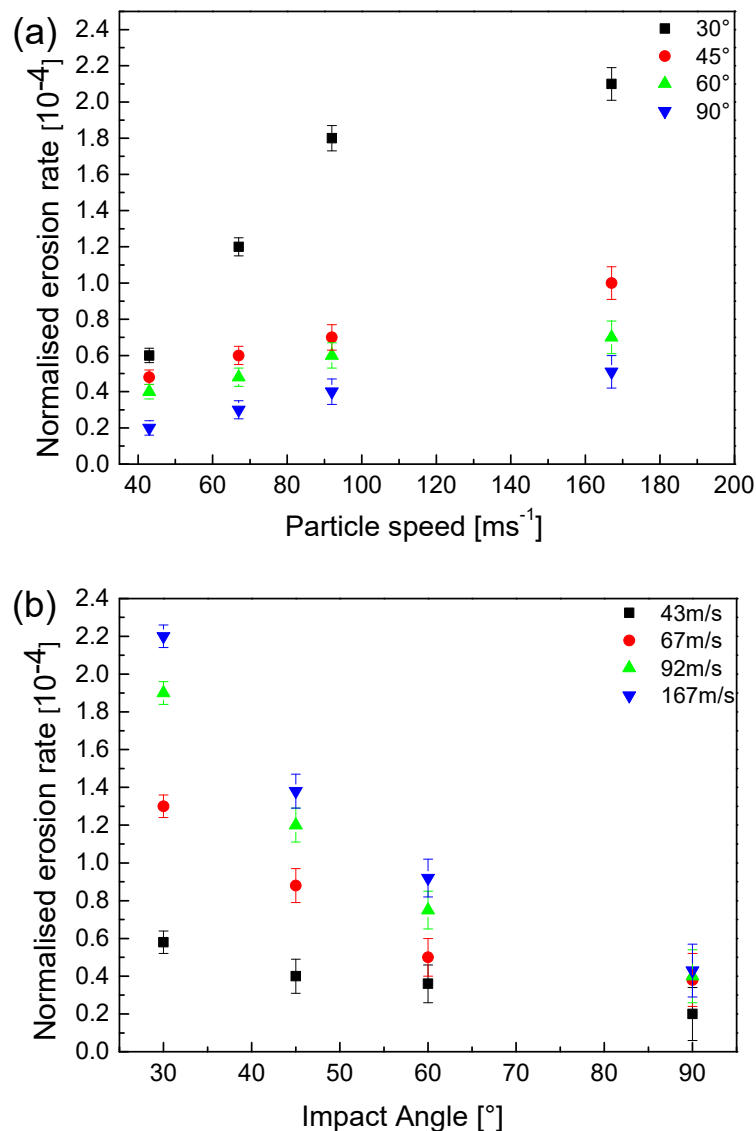


Figure 5. Normalized erosion rate vs. (a) particle speed and (b) impact angle. Error bars indicates 1 sigma scatter.

Figures 6–9 show the morphology of the API X120 target metal surfaces subjected to erosion under various impact angles and particle speeds. Clearly, the surface morphology of the eroded target metal is influenced by particle speed and impact angle. Different combinations of impact angle and particle speed induced different erosion mechanisms in predominance. This is presumably due to the changing magnitude of momentum vector on the target metal surface that led to the changes in the interaction between the target metal and the impinging particles. Table 2 summarizes the predominant morphological changes observed on the eroded metal surfaces at various combinations of angular impact and particle speed.

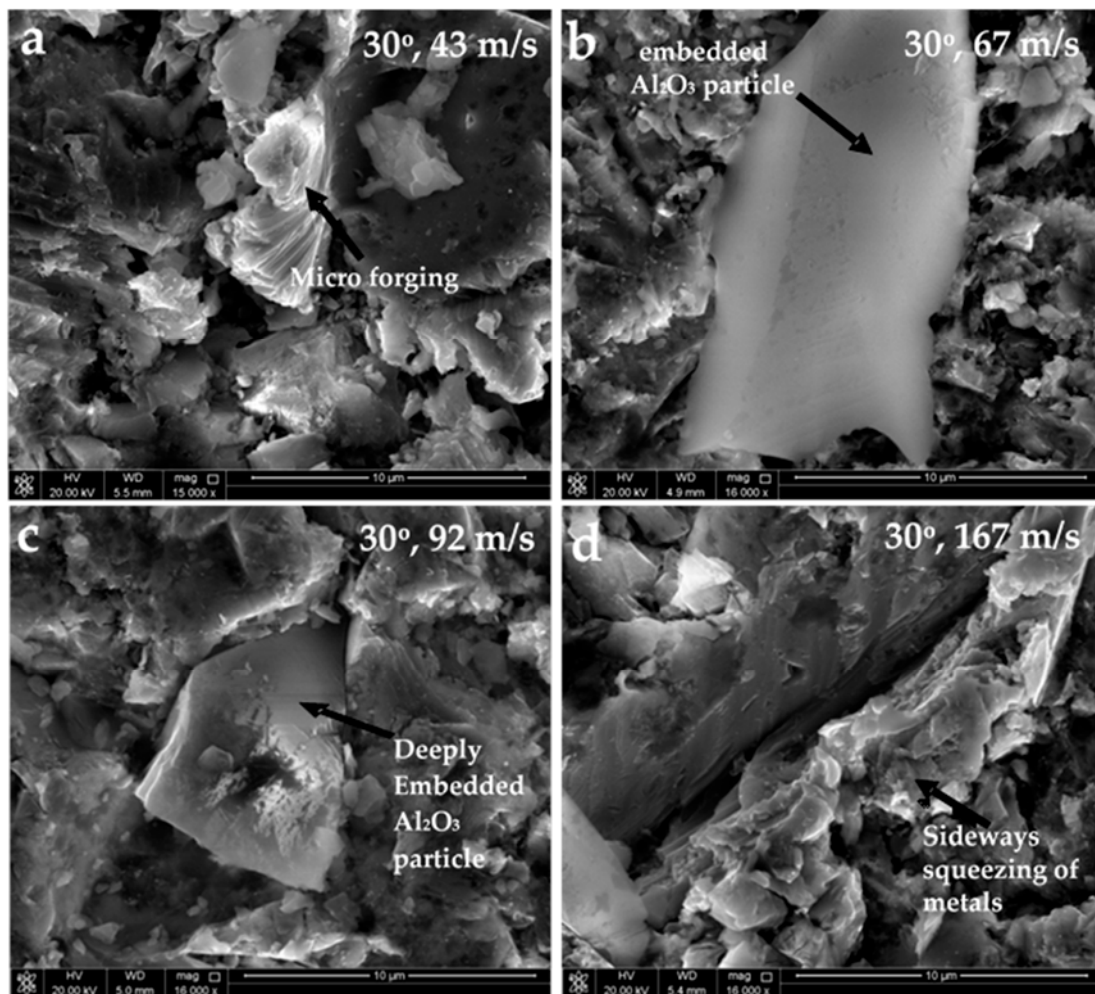


Figure 6. SEM micrograph of steel specimen after erosion at 30° impact angle and different particle speeds of (a) 43 m·s⁻¹, (b) 67 m·s⁻¹, (c) 92 m·s⁻¹, (d) 167 m·s⁻¹.

At lower impact angles (e.g., 30°, 45°) and lower particle speed (e.g., 43 m·s⁻¹), the target steel specimen is plastically deformed as a result of micro-forging was observed. Examples of micro-forging are shown in Figures 6a and 7a. At relatively higher speeds (e.g., 67 and 92 m·s⁻¹), occasional superficial embedment of the aluminum oxide particles onto the target metal surface were noticed (Figure 6b,c). Under similar conditions, similar types of features have been reported for AISI 1018 steel [33]. Superficial embedment of aluminum oxide particle on the target steel surface at lower particle speeds has been pointed out in other studies [41,42] where the phenomena were attributed to low kinetic energy of the bombarding particles [38,43]. At lower impact angles (e.g., 30°), when the particle speed increased to 192 m·s⁻¹, ploughing marks at the metal surface were prominent. The erodent particles appeared to create grooves with material piled up on the sides, as evident in Figure 6d. The erosion mechanism observed at lower impact angles (30°, 45°) is in agreement with the observation of Juan et al. [44], who reported similar erosion mechanism for AISI 1018 at lower impact angles. In agreement with the present work, other works [12] also suggested micro-forging and plastic deformation to be the prevalent material removal mechanisms at 30° impact angle.

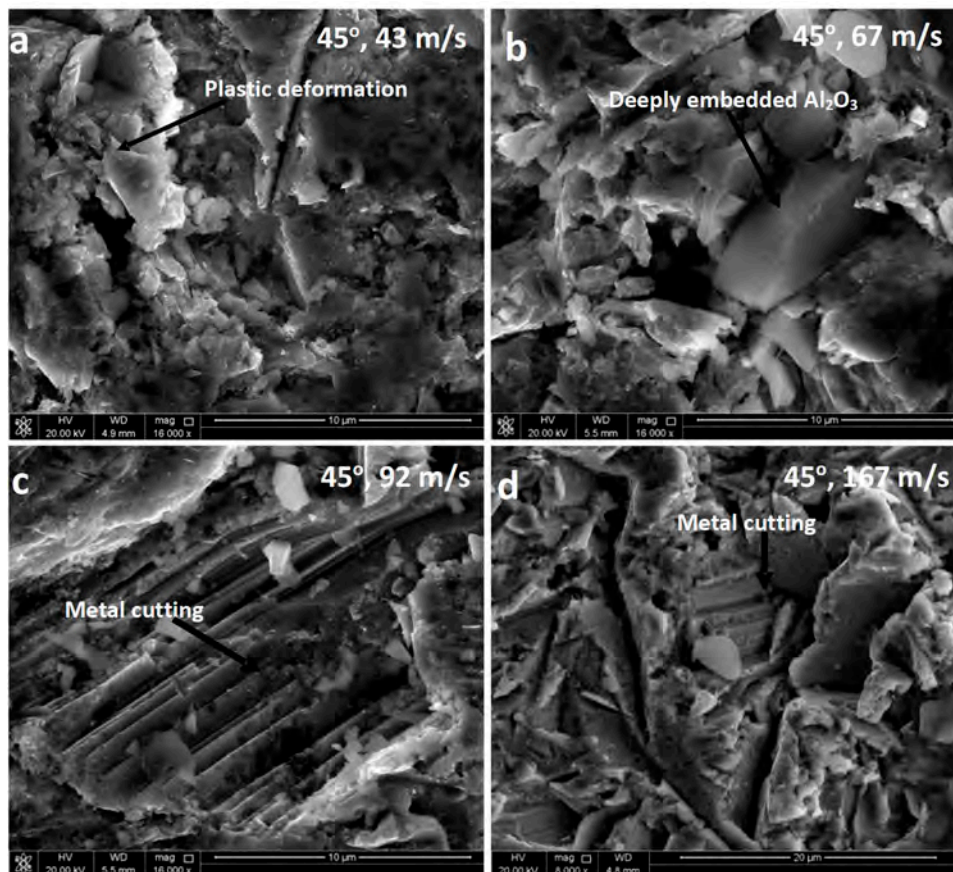


Figure 7. SEM micrograph of steel specimen after erosion at 45° impact angle and different particle speeds of (a) 43 m·s⁻¹, (b) 67 m·s⁻¹, (c) 92 m·s⁻¹, (d) 167 m·s⁻¹.

Flattening of the piled up materials lip at the side of the grooves was observed at all impact angles, generally at a higher speed. This is considered as the result of continuous bombardment of the target specimen by the erodent particle (examples shown in Figures 6d, 8d and 9d). Presumably, at higher particle speeds, the horizontal component of kinetic energy associated with the impinging particles is responsible for the ploughing mechanism. In our earlier work [34], under similar conditions, occurrence of ploughing was observed during the erosion of API X42 steel. At relatively higher impact angles (e.g., 60°) and a higher particle velocity (e.g., 167 m·s⁻¹), apart from the random ploughing mark, flattening of the preformed groove were observed as a common feature, as shown in Figure 8d. This phenomenon can be ascribed to the continuous bombardment of the target steel surface by increasing the number of high speed aluminum oxide particles. The flattening marks are presumed to be caused by stacking the layers of deformed aluminum oxide on the eroded steel surface, as reported by Brainard and Salik [45].

Unlike the ordinary pipeline steels, for API X120 at 30° impact angle metal-cutting was not commonly observed even at the highest particle speed. This is presumed due to its novel microstructure and relatively higher hardness, which did not allow the impinging particles to reach deep enough into the material to generate the cutting marks. As the angle of impact increased to 45°, micro-forging was observed on the metal surface at 43 m·s⁻¹ (Figure 7a) which is in agreement with the observation of Clark and Wong [30] as well as Alam et al. [46]. In addition, at 45° impact angle, at higher particle speeds (67–167 m·s⁻¹), features like deep level embedment of the erodent particles (Figure 7b), metal cutting (Figure 7c,d) were also observed. Appearance of deep level embedment of the erodent particles at higher impact angles can be argued to be the result of the higher values of the vertical components of particle momentum forcing the impinging particle to go deeper into the target metal. Examples of deep level embedment at higher impact angles are shown in Figures 7b, 8b and 9c. Apart from the

deep level embedment of particles at relatively higher impact angles (e.g., 45° , 60°), metal cutting has been observed as a prominent mechanism of erosion at relatively higher particle speeds ($\geq 92 \text{ m}\cdot\text{s}^{-1}$). In combinations of higher impact angles and higher particle speeds, the solid erodent particles the acquired required critical velocity to cut the metal into the form of small metallic chips. Examples of metal-cutting have been shown in Figure 7c,d, Figures 8c and 9c. At 45° and 60° impact angles, under higher speeds, metal-cutting was very common since both vertical component and horizontal component of the particle velocity were significantly high to force the erodent particle go relatively deeper into the target metal and at the same time to move them laterally further, resulting the phenomena of metal cutting. However, the metal-cutting observed at 90° impact angle is assumed to be a random. At 90° impact angle, ideally there should be no horizontal component of the velocity vector which can drag the particle through the metal laterally. At 90° impact angle, the incoming particles are likely to hit the metal surface vertically which can only make the particle go further deeper into the target metal. Therefore, whatever small amount of metal-cutting observed at 90° impact angle is assumed to be the result of scattered movement of some of the erodent particles which perhaps hit the particle at angles less than 90° and thus had a horizontal component of the velocity vector which might have dragged the particle laterally on the target metal. It is also possible that the rebound particles collided with the incoming particles resulting in a deflection of the original trajectories of the incoming particles. These deflected erodent particles again impacted the target steel surface at an acute angle resulting in metal cutting [32]. Similar mechanism was reported in previous work for other pipeline steels [46,47].

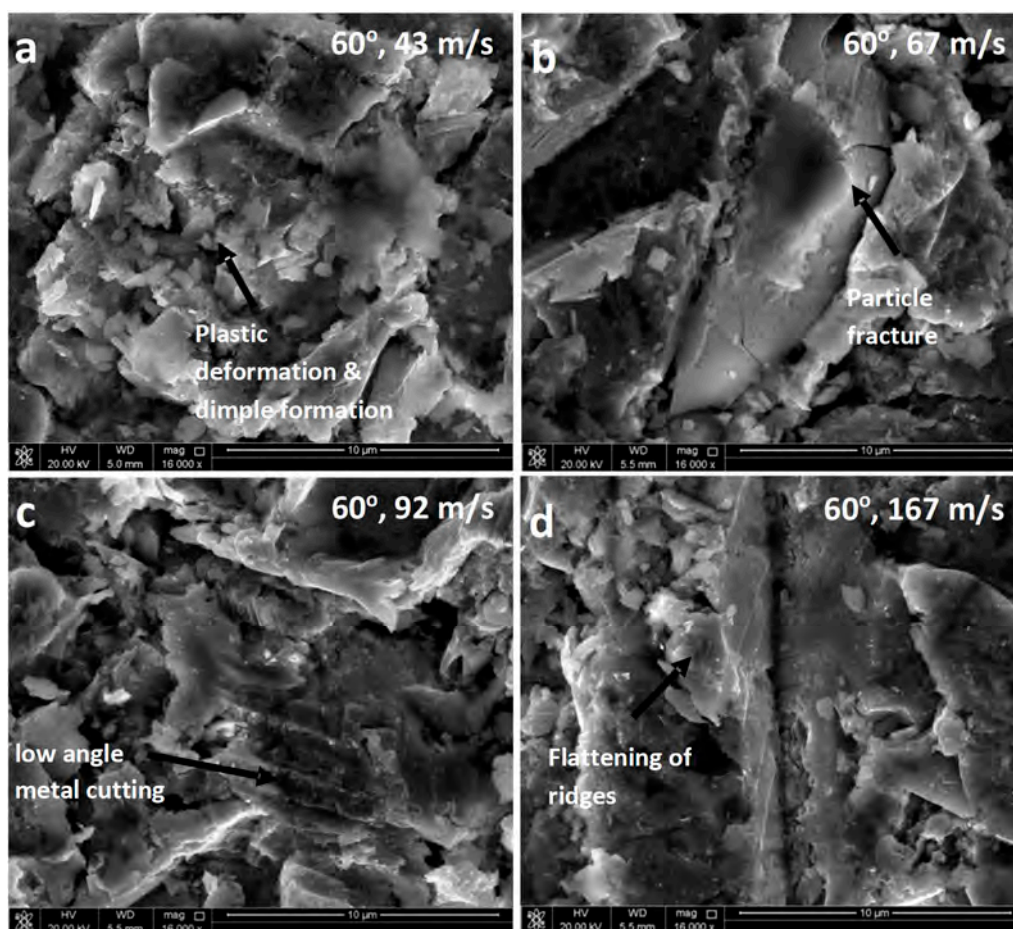


Figure 8. SEM micrograph of steel specimen after erosion at 60° impact angle and different particle speeds of (a) $43 \text{ m}\cdot\text{s}^{-1}$, (b) $67 \text{ m}\cdot\text{s}^{-1}$, (c) $92 \text{ m}\cdot\text{s}^{-1}$, (d) $167 \text{ m}\cdot\text{s}^{-1}$.

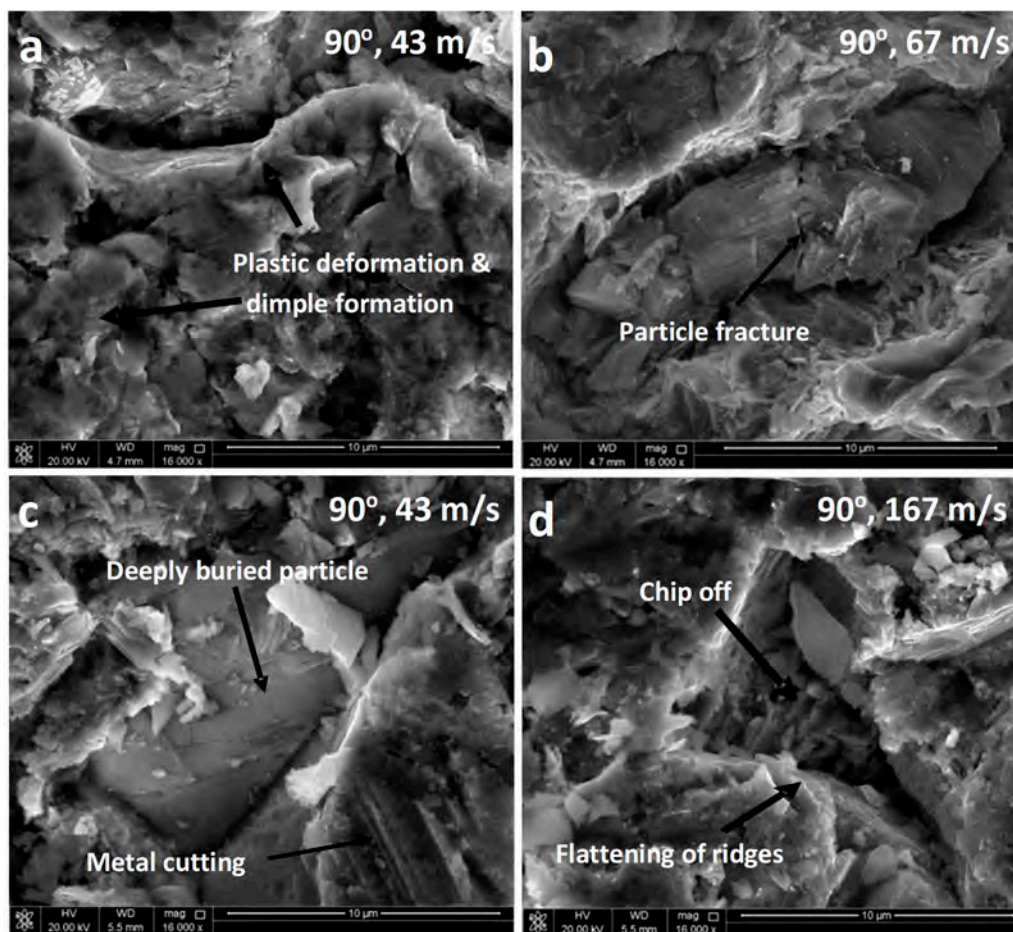


Figure 9. SEM micrograph of steel specimen after erosion at 90° impact angle and different particle speeds of (a) $43 \text{ m}\cdot\text{s}^{-1}$, (b) $67 \text{ m}\cdot\text{s}^{-1}$, (c) $92 \text{ m}\cdot\text{s}^{-1}$, (d) $167 \text{ m}\cdot\text{s}^{-1}$.

In addition to the above-mentioned erosion mechanisms, at relatively a higher impact angle (e.g., $\geq 60^\circ$), SEM micrographs also revealed plastic deformation at relatively lower speeds (e.g., $43 \text{ m}\cdot\text{s}^{-1}$). At lower speeds, the erodent particle could only induce a relatively localized shear as a result of plastic deformation and dimple formation were observed. For example, at 90° impact angle and $43 \text{ m}\cdot\text{s}^{-1}$ particle speed, plastic deformation and associated dimple formation were observed (Figure 9a). Under the combination of relatively higher impact angles and lower particle speeds, Islam and Farahat [42] indicated initial work-hardening of target steel surface by the continuous bombardment of solid particles, which upon further bombardment of impinging acquires micro-crack. On the other hand, at higher angular impact when the particle speed is relatively higher (e.g., $67 \text{ m}\cdot\text{s}^{-1}$), embedded aluminum oxide particle underwent fracture (Figure 9b) due to the continuous bombardment of the incoming erodent particles. At further higher speeds (e.g., $92 \text{ m}\cdot\text{s}^{-1}$), upon receiving further strikes from incoming erodent particle, the embedded aluminum oxide particles were cracked and went deeper into the target metal, as is observed in Figure 9c. With even higher speed (i.e., $167 \text{ m}\cdot\text{s}^{-1}$), the fractured particles were occasionally observed chipped off from creating the formation of a surface-void and leaving the metal surface with vulnerable lips (Figure 9d). It was noticed similar qualitative erosion characteristics for other pipeline steels in our earlier works [8,32,33,47]. Any further increase in particle speed could have had resulted in different erosion mechanisms as indicated elsewhere [29,38,47]. It is generally believed that at higher impact angles and higher particle speeds, the elastic strain energy is high enough and exceed the strain energy of the target materials [43,48]. At higher impact angles the impinging and reflecting aluminum oxide particles may collide and change the trajectory of the impinging particles; and this could result in ploughing of the target steel surface [49,50].

On a qualitative level, EDX of samples under most exposure conditions indicated a transfer of aluminum oxide particles to the target metal. The presence of aluminum oxide in the target metal is indicated by the presence of aluminum (Al) peak which was not observed in case of unexposed (uneroded) steel. Figure 10a shows the EDX spectrum of the unexposed target metal; and Figure 10b shows the representative EDX spectrum of the eroded target metal.

On a qualitative level, API X120 steel did not show much difference in the morphologies of the eroded surface compared to the other pipeline steels under similar exposure conditions. However, profilometric data revealed that, the penetration depth is 1520% less compared to the other pipeline steels. In addition, weight loss percentage and erosion rate for API X120 steel have been observed to be respectively ~10% and ~20% less compared to API X100 [23] and AISI 1018 [33] under similar exposure conditions. Higher erosion resistance of API X120 steel is presumably due to the higher hardness originated from its salient microstructure which certainly needs further investigation and is one of our future objectives. Due to the different chemical composition of this steel, under similar heat treatment conditions, API X120 is likely to gain a greater hardness. Moreover, because of the existence of alloying elements such as Ni and Cr, it is amenable to achieve microstructure of higher hardness and strength by modulating the heat treatment process of this steel.

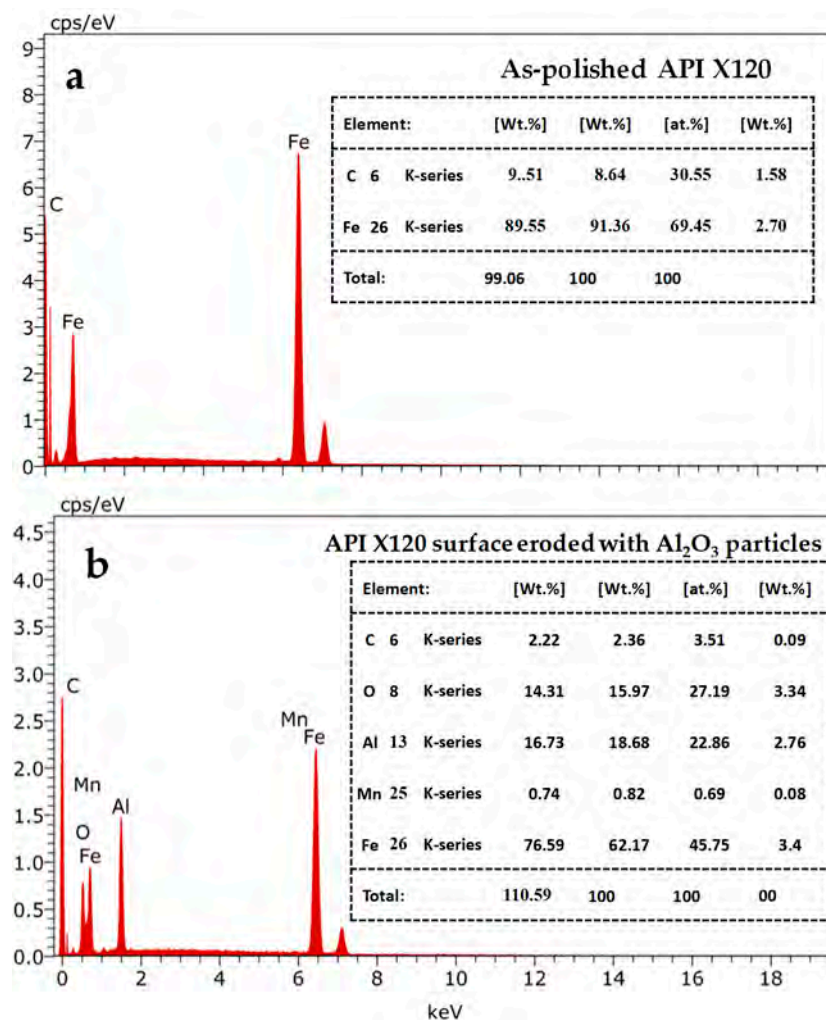


Figure 10. Representative EDX characteristics of API X120 samples (a) as-polished (unexposed), (b) subjected to erosive interaction with aluminum oxide particles and observed at all combinations of impact angles and particle speeds.

4. Conclusions

The erosion behaviour of API X120 steel has been investigated using aluminum oxide as erodent particle under simulated erosive environment inside the pipelines, with an objective to introduce a better understanding of erosion behavior of this cutting-edge pipeline steel. The effects of various combinations of particles speed and impact angle on the erosion behaviour of API X120 pipeline steel is presented. The weight loss and erosion rate increased with increasing particle speed for all the impact angles due to the high kinetic energy by the erodent particles. The weight loss and erosion rate have been found the maximum at the lowest angular impact (30°) and generally decreased with increasing impact angle, indicating that the materials loss as a result of the erosion process is the maximum at relatively lower impact angles where plastic deformation, micro-forging and metal-cutting have been observed the predominant mechanisms of erosion as revealed with SEM. Increasing particles speed generally amplified the erosion of metal surface via micro-cutting while increase in impact angle resulted in deeper embedment of erodent particles with relatively less material loss. Finally, combination of higher particle speed and higher impact angle confirmed the occurrence of ploughing and flattening of the preformed groove as the dominant erosion mechanism. The results obtained in this work suggest that, like the other pipeline steels, the erosion behaviour of the API X120 steel can also be strongly influenced by solid particle speed, impact angle and material property. However, the overall erosion resistance of this steel in terms of particle penetration depth, weight-loss and erosion rate is appreciably higher compared to many other grades of pipeline steels that were used for our previous studies. The results obtained in this study are likely to be useful for designing high efficient pipelines in varieties of erosive environments.

Author Contributions: R.A.S. planned and designed the experiments. P.C.O. and M.H.S. (Mostafa H. Sliem) conducted erosion experiments at various impact angles and particulate speeds. A.M.A. and R.K. assisted in analyzing the samples using SEM/EDX and Profilometer respectively. M.H.S. (Mobbassar Hassan Sk) and A.M.A.M. prepared the initial draft of the manuscript. R.A.S. prepared the final draft of the manuscript.

Funding: This research was funded by NPRP from the Qatar National Research Fund (a member of the Qatar Foundation) (No. 9-080-2-039).

Acknowledgments: Authors greatly acknowledge the technical support of the Center for Advanced Materials (CAM), Qatar University.

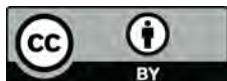
Conflicts of Interest: The authors declare no conflict of interest.

References

1. Ríos-Mercado, R.Z.; Borraz-Sánchez, C. Optimization problems in natural gas transportation systems: A state-of-the-art review. *Appl. Energy* **2015**, *147*, 536–555. [[CrossRef](#)]
2. Herrán, A.; de la Cruz, J.M.; de Andrés, B. A mathematical model for planning transportation of multiple petroleum products in a multi-pipeline system. *Comput. Chem. Eng.* **2010**, *34*, 401–413. [[CrossRef](#)]
3. Herrán, A.; de la Cruz, J.M.; de Andrés, B. Global Search Metaheuristics for planning transportation of multiple petroleum products in a multi-pipeline system. *Comput. Chem. Eng.* **2012**, *37*, 248–261. [[CrossRef](#)]
4. Jones, N.N.; Birch, R.S. Influence of internal pressure on the impact behavior of steel pipelines. *J. Press. Vessel Technol.* **1996**, *118*, 464–471. [[CrossRef](#)]
5. Igi, S.; Sakimoto, T.; Endo, S. Effect of internal pressure on tensile strain capacity of X80 pipeline. *Procedia Eng.* **2011**, *10*, 1451–1456. [[CrossRef](#)]
6. Wood, R.J.K.; Jones, T.F. Investigations of sand-water induced erosive wear of AISI 304L stainless steel pipes by pilot-scale and laboratory-scale testing. *Wear* **2003**, *255*, 206–218. [[CrossRef](#)]
7. Hu, X.; Neville, A. CO₂ erosion-corrosion of pipeline steel (API X65) in oil and gas conditions—A systematic approach. *Wear* **2009**, *267*, 2027–2032. [[CrossRef](#)]
8. Paul, O.; Mohamed, A.M.A. Erosion-corrosion in oil and gas industry: A review. *Int. J. Met. Mater. Sci. Eng.* **2014**, *4*, 7–28.
9. Mohtadi-Bonab, M.A.; Szpunar, J.A.; Razavi-Tousi, S.S. A comparative study of hydrogen induced cracking behavior in API 5L X60 and X70 pipeline steels. *Eng. Fail. Anal.* **2013**, *33*, 163–175. [[CrossRef](#)]

10. Andrews, N.; Giourntas, L.; Galloway, A.M.; Pearson, A. Effect of impact angle on the slurry erosion-corrosion of Stellite 6 and SS316. *Wear* **2014**, *320*, 143–151. [[CrossRef](#)]
11. Wood, R.J.K.; Walker, J.C.; Harvey, T.J.; Wang, S.; Rajahram, S.S. Influence of microstructure on the erosion and erosion-corrosion characteristics of 316 stainless steel. *Wear* **2013**, *306*, 254–262. [[CrossRef](#)]
12. Manisekaran, T.; Kamaraj, M.; Sharrif, S.M.; Joshi, S.V. Slurry erosion studies on surface modified 13Cr-4Ni Steels: Effect of angle of impingement and particle size. *J. Mater. Eng. Perform.* **2007**, *16*, 567–572. [[CrossRef](#)]
13. López, D.; Congote, J.P.; Cano, J.R.; Toro, A.; Tschiptschin, A.P. Effect of particle velocity and impact angle on the corrosion-erosion of AISI 304 and AISI 420 stainless steels. *Wear* **2005**, *259*, 118–124. [[CrossRef](#)]
14. Chauhan, A.K.; Goel, D.B.; Prakash, S. Solid particle erosion behaviour of 13Cr-4Ni and 21Cr-4Ni-N steels. *J. Alloys Compd.* **2009**, *467*, 459–464. [[CrossRef](#)]
15. Burstein, G.T.; Sasaki, K. Effect of impact angle on the slurry erosion-corrosion of 304L stainless steel. *Wear* **2000**, *240*, 80–94. [[CrossRef](#)]
16. Matsumura, M.; Oka, Y.; Hiura, H.; Yano, M. The role of passivating film in preventing slurry erosion-corrosion of austenitic stainless steel. *ISIJ Int.* **1991**, *31*, 168–176. [[CrossRef](#)]
17. Levy, A.V. The solid particle erosion behavior of steel as a function of microstructure. *Wear* **1981**, *68*, 269–287. [[CrossRef](#)]
18. Green, G.M.; Taggart, R.; Polonis, D.H. Influence of microstructure on the erosion of plain carbon steels. *Metallography* **1981**, *14*, 191–212. [[CrossRef](#)]
19. Liebhard, M.; Levy, A. The effect of erodent particle characteristics on the erosion of metals. *Wear* **1991**, *151*, 381–390. [[CrossRef](#)]
20. Tilly, G.P.; Sage, W. The interaction of particle and material behaviour in erosion processes. *Wear* **1970**, *16*, 447–465. [[CrossRef](#)]
21. Choi, B.W.; Seo, D.H.; Jang, J.I. A nanoindentation study on the micromechanical characteristics of API X100 pipeline steel. *Met. Mater. Int.* **2009**, *15*, 373–378. [[CrossRef](#)]
22. Zhao, M.C.; Yang, K.; Shan, Y. The effects of thermo-mechanical control process on microstructures and mechanical properties of a commercial pipeline steel. *Mater. Sci. Eng. A* **2002**, *335*, 14–20. [[CrossRef](#)]
23. Liu, L.; Xiao, H.; Li, Q.; Liu, Y.; Li, P.; Yang, Z.; Yu, H. Evaluation of the fracture toughness of X70 pipeline steel with ferrite-bainite microstructure. *Mater. Sci. Eng. A* **2017**, *688*, 388–395.
24. Lu, S.H.; Ling, X.; Zhang, J.C. Investigate on the properties of X80 pipeline steel damaged by high temperature. *Procedia Eng.* **2015**, *130*, 609–616. [[CrossRef](#)]
25. Okonkwo, P.C.; Shakoor, R.A.; Zagho, M.M.; Mohamed, A.M.A. Erosion behaviour of API X100 pipeline steel at various impact angles and particle speeds. *Metals* **2016**, *6*, 232. [[CrossRef](#)]
26. Fairchild, D.P.; Macia, M.L.; Bangaru, N.V.; Koo, J.Y. Girth welding development for X120 line pipe. In Proceedings of the Thirteenth International Offshore and Polar Engineering Conference, Honolulu, HI, USA, 25–30 May 2003.
27. Tanguy, B.; Luu, T.T.; Perrin, G.; Pineau, A.; Besson, J. Plastic and damage behaviour of a high strength X100 pipeline steel: Experiments and modelling. *Int. J. Press. Vessels Pip.* **2008**, *85*, 322–335. [[CrossRef](#)]
28. *ASTM G76-13 Standard Test Method for Conducting Erosion Tests by Solid Particle Impingement Using Gas Jets*; ASTM International: West Conshohocken, PA, USA, 2013.
29. Ruff, A.W.; Ives, L.K. Measurement of solid particle velocity in erosion wear. *Wear* **1975**, *35*, 195–199. [[CrossRef](#)]
30. Clark, H.M.; Wong, K.K. Impact angle, particle energy and mass loss in erosion by dilute slurries. *Wear* **1995**, *186–187*, 454–464. [[CrossRef](#)]
31. Chen, S.L.; Siitonen, P.; Kettunen, P. A method for measuring particle velocity in thermal spraying. *Surf. Coat. Technol.* **1994**, *64*, 17–20. [[CrossRef](#)]
32. Okonkwo, P.C.; Mohamed, A.M.A. Erosion mechanisms of API X42 and AISI 1018 steel materials at normal impact angle. *Int. J. Eng. Sci. Innov. Technol.* **2014**, *3*, 402–407.
33. Paul, C.O.; Mohamed, A.M.A.; Ahmed, E. Influence of particle velocities and impact angles on the erosion mechanisms of AISI 1018 steel. *Adv. Mater. Lett.* **2015**, *6*, 653–659.
34. Okonkwo, P.C.; Shakoor, R.A.; Ahmed, E.; Mohamed, A.M.A. Erosive wear performance of API X42 pipeline steel. *Eng. Fail. Anal.* **2016**, *60*, 86–95. [[CrossRef](#)]
35. Axinte, D.A.; Srinivasu, D.S.; Kong, M.C.; Butler-Smith, P.W. Abrasive waterjet cutting of polycrystalline diamond: A preliminary investigation. *Int. J. Mach. Tools Manuf.* **2009**, *49*, 797–803. [[CrossRef](#)]

36. Söderberg, S.; Hogmark, S.; Swahn, H. Mechanisms of material removal during erosion of a stainless steel. *ASLE Trans.* **1983**, *26*, 161–172. [[CrossRef](#)]
37. Hutchings, I.M.; Winter, R.E.; Field, J.E. Solid particle erosion of metals: The removal of surface material by spherical projectiles. *Proc. R. Soc. A* **1976**, *348*, 379–392. [[CrossRef](#)]
38. Al-Bukhaiti, M.A.; Ahmed, S.M.; Badran, F.M.F.; Emara, K.M. Effect of impingement angle on slurry erosion behaviour and mechanisms of 1017 steel and high-chromium white cast iron. *Wear* **2007**, *262*, 1187–1198. [[CrossRef](#)]
39. Hutchings, I.M.; Winter, R.E. Particle erosion of ductile metals: A mechanism of material removal. *Wear* **1974**, *27*, 121–128. [[CrossRef](#)]
40. Cai, F.; Huang, X.; Yang, Q. Mechanical properties, sliding wear and solid particle erosion behaviors of plasma enhanced magnetron sputtering CrSiCN coating systems. *Wear* **2015**, *324–325*, 27–35. [[CrossRef](#)]
41. Hutchings, I.M. A model for the erosion of metals by spherical particles at normal incidence. *Wear* **1981**, *70*, 269–281. [[CrossRef](#)]
42. Islam, M.A.; Farhat, Z.N. Effect of impact angle and velocity on erosion of API X42 pipeline steel under high abrasive feed rate. *Wear* **2014**, *311*, 180–190. [[CrossRef](#)]
43. Hutchings, I.M. Deformation of metal surfaces by the oblique impact of square plates. *Int. J. Mech. Sci.* **1977**, *19*, 45–52. [[CrossRef](#)]
44. Juan, R.L.C.; Vite-Torres, M.; Gallardo-Hernandez, E.A.; Vera-Cardenas, E.E. Solid particle erosion on different metallic materials. *Tribol. Int.* **2013**, *5*, 63–78.
45. Brainard, W.A.; Salik, J. An investigation into the role of adhesion in the erosion of ductile metals. *ASLE Trans.* **1981**, *24*, 302–306. [[CrossRef](#)]
46. Alam, T.; Islam, M.A.; Farhat, Z.N. Slurry erosion of pipeline steel: Effect of velocity and microstructure. *J. Tribol.* **2015**, *138*, 021604. [[CrossRef](#)]
47. Islam, M.A.; Alam, T.; Farhat, Z.N.; Mohamed, A.; Alfantazi, A. Effect of microstructure on the erosion behavior of carbon steel. *Wear* **2015**, *332–333*, 1080–1089. [[CrossRef](#)]
48. Sundararajan, G.; Shewmon, P.G. A new model for the erosion of metals at normal incidence. *Wear* **1983**, *84*, 237–258. [[CrossRef](#)]
49. Gomes-Ferreira, C.; Ciampini, D.; Papini, M. The effect of inter-particle collisions in erosive streams on the distribution of energy flux incident to a flat surface. *Tribol. Int.* **2004**, *37*, 791–807. [[CrossRef](#)]
50. Shirazi, S.A.; McLaury, B.S. Erosion modeling of elbows in multiphase flow. In Proceedings of the 2000 ASME Fluids Engineering Summer Meeting, Boston, MA, USA, 11–15 June 2000; p. 11251.



© 2018 by the authors. Licensee MDPI, Basel, Switzerland. This article is an open access article distributed under the terms and conditions of the Creative Commons Attribution (CC BY) license (<http://creativecommons.org/licenses/by/4.0/>).